Transp Porous Med (2018) 124:183–201
https://doi.org/10.1007/s11242-018-1058-6

Insight into Heterogeneity Effects in Methane Hydrate Dissociation via Pore-Scale Modeling

S. M. Abdoli[1] · S. Shafiei[1] · A. Raoof[2] · A. Ebadi[1] · Y. Jafarzadeh[1]

Received: 2 January 2018 / Accepted: 5 April 2018 / Published online: 23 April 2018

Abstract The production of natural gas from the gas hydrates has attracted significant attention over the last few decades. A continued challenge in gas hydrates is the estimation of the stored gas capacity. To alleviate this problem, this study uses the numerical modeling to provide insight into the distribution of hydrate in porous media and to obtain information about the application of high pressure for gas recovery. Hydrate dissociation process in porous media is modeled at the pore scale using pore network modeling by considering the uniform and non-uniform hydrate distribution. We explored the effect of gas clustering, saturation, and recovery, and their dependency on the underlying parameters including the pore size distribution, the applied pressure drops across the pore structures, and the initial hydrate saturation. We found that non-uniform hydrate distribution, larger pore sizes along with high-pressure drop, and higher initial hydrate saturations enhanced gas release. Additionally, our results confirmed the findings of the previous studies using 2D networks which studied pressure drop during hydrate dissociation in reservoirs.

Keywords Hydrate · Dissociation · Depressurization · Pore network model · Porous media

List of symbols

N_H	Theoretical hydration number
R_{pi}	Radius of pore i
R_{max}	Maximum radius
R_{min}	Minimum radius
x_i	A random number between zero and one
ε_i	Hydrate fraction in pore i

✉ S. Shafiei
ssirous@yahoo.com

[1] Faculty of Chemical Engineering, Sahand University of Technology, Tabriz, Iran

[2] Department of Earth Science, Utrecht University, Utrecht, The Netherlands

β_{D}	Distribution parameter
V_{hi}	Volume of hydrate in pore i
S_{H}^{0}	Initial hydrate saturation
F_{ij}	Flow rate in throat ij
ΔP_{ij}	Pressure difference of throat ij
R_{ij}	Resistance to flow of throat ij
μ_{l}	Dynamic viscosity of the liquid
l_{ij}	Length of throat ij
r_{ij}	Radius of throat ij
G	Sparse matrix
P	Vector of unknown pressure
b	Known vector
Π_{ij}	Threshold pressure
P_{c}^{ij}	Capillary pressure of throat ij
P_{l}^{j}	Pressure of pore j
σ	Interfacial tension
P_{g}	Gas pressure
z	Compressibility factor
n	Number of mole
R	Gas constant
T	Temperature
V	Volume
η	Gas recovery yield
n_1	Amount of initial gas
n_2	Amount of final gas
B	A dimensionless flow resistance factor
π	Pi number
$A_{\mathrm{w},ij}$	Cross-sectional area for wet phase
r_{m}	Inscribed radius
S_{f}	Dimensionless shape factor
A	Area
P	Perimeter
$F(\alpha)$	A corner angularity factor
α	Angularity
k	Absolute permeability
K_{r}	Relative permeability
Np	Number of pores in each direction of the network

1 Introduction

The increasing population of the world and the associated energy consumption creates a demand for resources such as oil, coal, and natural gas (Asif and Muneer 2007; Shafiee and Topal 2009). Combustion of CH_4 produces less CO_2 compared to oil and coal, which suggests natural gas as a cleaner energy supply (Cherskii and Bondarev 1972; Collett 1992; Englezos and Lee 2005). On the other hand, CH_4 is environmentally considered as a cause for global warming (Mestdagh et al. 2017; Moss et al. 2000; Ruppel and Kessler 2017). Therefore, reducing methane emission helps to prevent the climate tipping and environmental impacts

(Cao et al. 1998). Methane can be found in the form of gas hydrate. There, the amount of trapped methane is 100 times higher compared to its storage capacity in the conventional gas reserves (Collett et al. 2000; Collett and Kuuskraa 1998; Paull and Dillon 2001). For example, with dissociation of 1 m^3 hydrate, approximately 160 m^3 CH_4 and 1 m^3 of H_2O at standard temperature and pressure conditions (STP) are produced (Max and Dillon 1998). Therefore, gas hydrates are considered as a potential source of natural gas (Bhade and Phirani 2015; Boswell and Collett 2011; Collett et al. 2009; Makogon 2010; Makogon et al. 2007; Max and Lowrie 1996; Merey and Sinayuc 2016; Reagan et al. 2015).

Natural gas hydrates are crystalline, ice-like compounds that are formed under high-pressure and low-temperature conditions (Dendy Sloan 1998). Temperature and pressure together with the initial hydrate content are the key factors that control capacity for hydrate dissociation in reservoirs. Depressurization, thermal stimulation, and inhibitor injection are among natural gas production methods in the hydrate reservoirs which are based on altering the thermodynamic equilibrium (Dendy Sloan 1998; Li et al. 2016). The most common method is depressurization. In this method, the pressure of the reservoir is reduced, at a constant temperature, to below the equilibrium pressure of the hydrate [Fig. 1a—path (1)]. In thermal stimulation method, the temperature of hydrate reservoir is increased above the equilibrium temperature of the hydrate at constant pressure [Fig. 1a—path (2)]. Eventually, for the case of inhibitor injection method, often methanol or brine is injected into the reservoir with the purpose of fluctuating the thermodynamic equilibrium, and subsequently, the dissociation of the hydrate occurs [Fig. 1a—path (3)]. The least energy-intensive method is thought to be the depressurization method with the advantages of simplicity, technical feasibility, and continuous production (Hong and Pooladi-Darvish 2005; Moridis et al. 2009). Hence, in this paper, the depressurization method for decomposition of methane hydrate in porous media is studied.

Methane hydrate dissociation reaction can be described by Eq. (1) as:

$$CH_4 \cdot N_H\, H_2O(s) \rightarrow CH_4(g) + N_H\, H_2O(l) \tag{1}$$

where N_H is known as hydration number, which is defined as the ratio of water to gas in a hydrate molecule $CH_4 \cdot N_H H_2O$. The theoretical hydration number N_H is 5.75 (= 46/8), which means 8 molecules of methane gas are trapped in the cavity formed by 46 water molecules connected with hydrogen bonding (Dendy Sloan Jr. and Koh 2007). Experiments on a small scale in the laboratory for hydrate formation and dissociation are often conducted for liquid solutions missing the critical porous structure of the media (Bai et al. 2009). Pore size distribution, porosity, connectivity, and permeability of porous media are main parameters having influence on hydrate formation and dissociation (Han et al. 2017; Kumar et al. 2010; Uchida et al. 2002). So these parameters should be considered for the selection of the appropriate geometry of porous media.

Xu and Ruppel (1999) modeled gas hydrate system using analytical solution. They solved momentum, mass, and energy equation simultaneously. Davie and Buffett (2001), considering a continuum mixture of sediment, seawater, and hydrate, developed a numerical model to predict volume and distribution of gas hydrate in marine sediment. Sun et al. (2005) provided a thermal, three-phase, one-dimensional numerical model to simulate gas production from sediments containing methane hydrates by depressurization. They found that gas production is not very sensitive to the well temperature boundary condition. The finite element approximation technique is used by Cheng et al. (2013) for modeling of depressurization-induced gas production from a hydrate reservoir. Zhao et al. (2013) investigated gas production from hydrate deposits using a single vertical well by depressurization method. The cylindrical simulation system was utilized in their work. Myshakin et al. (2016) performed numerical

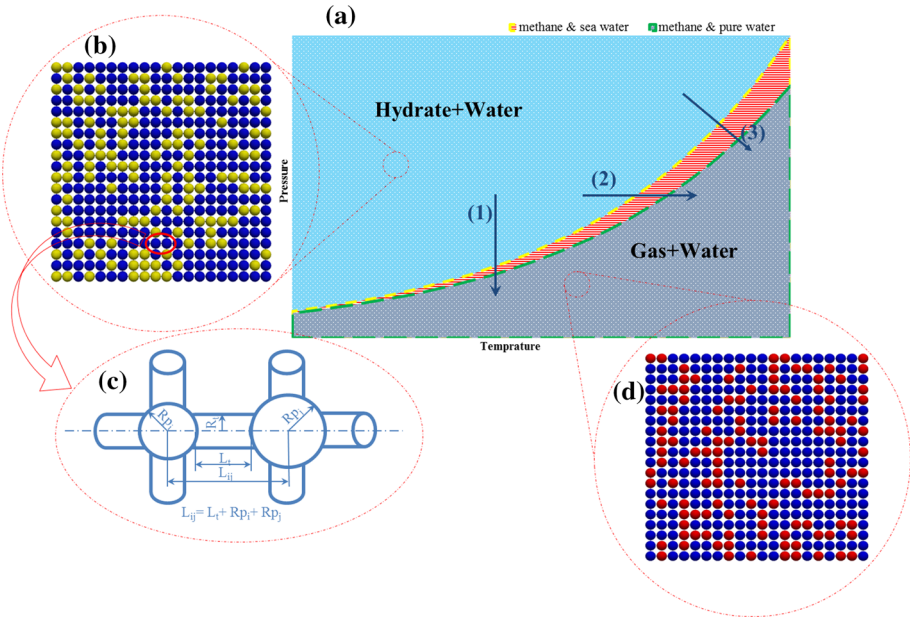

Fig. 1 **a** Schematic phase diagram showing the stability field of pressure and temperature for gas hydrates under varying thermodynamic conditions: (1) depressurization, (2) thermal stimulation, and (3) inhibitor injection. **b** Distribution of hydrate in regular 2D pore network model: yellow: hydrate; blue: water. **c** Schematic of two neighboring pores connected using a cylindrical throat. **d** Gas saturation in a 2D pore network model after depressurization method: red: gas; blue: water

simulations of gas production using a 3D reservoir model with depressurization method to estimate the production potential from hydrate-bearing sand units. In all of the mentioned models, the structural properties of porous media were ignored. Therefore, the hydrate reservoirs were assumed as continuous environment and the porosity coefficient was entered to the model equation as a constant parameter.

Recently, modeling strategies have been developed based on representing porous media's structural heterogeneity using pore network models allowing incorporation of pore size distribution and permeability. Tsimpanogiannis and Lichtner (2006) presented a two-dimensional pore network model based on invasion percolation. They studied the patterns obtained from the release of methane during the dissociation of methane hydrates without including dissociation kinetics caused by a sudden pressure reduction in the system below the hydrate equilibrium pressure. Liang et al. (2010) developed cubic pore network model to study the effect of hydrate particle formation and growth habit on the permeability. Jang and Santamarina (2011) investigated gas recovery and capillary-trapped residual gas saturation by simulating hydrate dissociation within pore networks. They defined a pore network model as a system of pores connected by zero-volume throats. Holtzman and Juanes (2011) examined the pressure evolution under thermally induced dissociation method by means of a pore-scale model. Tsimpanogiannis and Lichtner (2013) studied the gas saturation that resulted from dissociation of methane hydrate inside aqueous bulk or porous medium and then compared pore network results with the analytical solution. Mahabadi and Jang (2014) simulated gas expansion in a distributed hydrate system using a pore network model. 3D cubic network was used to evaluate gas saturation and relative permeability during gas production from hydrate

reservoirs by Jang and Santamarina (2014). Dai and Seol (2014) explored the relationship between apparent water permeability and hydrate saturation using 50×50 2D lattice pore network. Mahabadi et al. (2016) continued their previous work and identified water retention curve and relative permeability in hydrate-bearing sediments using pore network model simulation. Ai et al. (2017) proposed pore network models combined with X-ray computed tomography (CT) to analyze the permeability of gas hydrate system. However, the challenge still remains to determine how the interactions of structural heterogeneity of porous media and initial distribution of hydrate influence the gas clustering which leads to the methane production process from hydrate reservoirs.

This study is motivated by the need to expand predictive capabilities of hydrate decomposition processes. We have incorporated novel improvements on previously developed models of pore-scale hydrate dissociations which occur at the unsaturated pore networks. The specific objectives of this research are to: (1) apply a mechanistic modeling framework for hydrate dissociation via depressurization in porous media of different pore structures using 2D and 3D regular pore networks; (2) characterize the roles of structural heterogeneity and initial hydrate distribution on the gas saturation and calculation of the recovery efficiency; and (3) exploit the angular shape of pores and its effect on the recovery efficiency.

2 Modeling Procedure

In this study, we use the pore network modeling approach to represent the pore structure and to simulate the transport of the gas phase.

2.1 Representation of Porous Media Using Pore Network Model (Network Construction)

2.1.1 Geometry

At start, we use a 2D pore network with spherical pores and cylindrical throats, in which every pore is connected to 4 adjacent pores, i.e., coordination number is 4 for inner pores (Fig. 1c). Later, by increasing the pore coordination number to 6 the 3D cubic network is constructed. Ultimately, angular throats are used to represent the angularity of the pore structures within the network.

2.1.2 Characterization of Structure

For the construction of the network, the normal distribution function is used to obtain pore size as:

$$R_{\mathrm{pi}} = \left(R_{\mathrm{max}} - R_{\mathrm{min}}\right) * x_i + R_{\mathrm{min}} \tag{2}$$

where R_{min} and R_{max} are the minimum and maximum radii of pores and x_i is a random number between zero and one. The radius of each throat is chosen to be equal to half of minimum radius of the two adjacent pores connected to it.

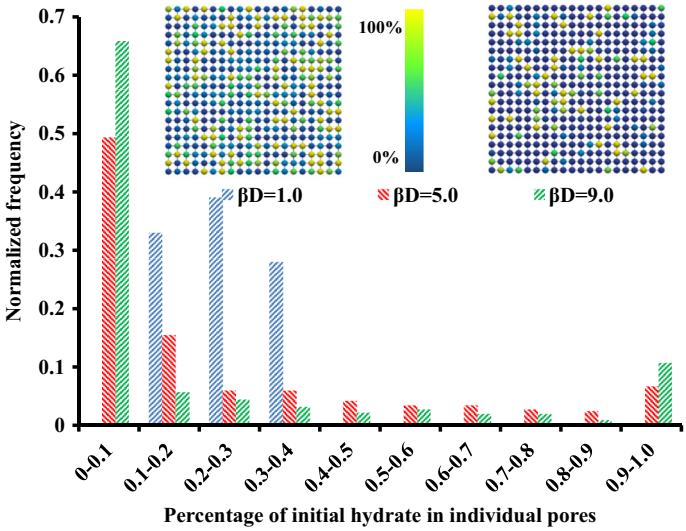

Fig. 2 Effect of β_D parameter on hydrate distribution in 2D pore network and schematic representation of hydrate distribution in network in $\beta_D = 1.0, 9.0$

2.2 Hydrate Distribution

We use a transformation method to control the non-uniform spatial distribution of hydrate within the network (Oliveira et al. 2011):

$$\varepsilon_i = \exp\left[\beta_D \left(x_i - 1\right)\right] \tag{3}$$

where x_i and β_D are a random number uniformly distributed in [0, 1) and distribution parameter, respectively, and ε_i is the hydrate fraction in pore i. In low degrees of hydrate saturation (i.e., 1–8%), we defined the $\frac{\varepsilon_i}{\sum_{j=1}^{N} \varepsilon_j}$, where N is the total number of pores, as a normalization factor for distribution in all pores.

The volume of hydrate in each pore can be calculated as:

$$V_{hi} = \frac{\varepsilon_i}{\sum_{j=1}^{N} \varepsilon_j} S_H^0 V \tag{4}$$

where V_{hi} is the volume of hydrate in each pore. S_H^0 and V are initial hydrate saturation and total volume of network, respectively. It is obvious that changing β_D in Eq. (3) affects the distribution of hydrate within the network. Figure 2 depicts the effect of β_D on hydrate distribution. By increasing β_D, distribution of hydrate becomes less uniform and, at the same time, a larger number of pores lack hydrate.

2.3 Obtaining the Pressure of Each Pore

Initially, all the pores are set to be filled with liquid water with some of them containing hydrates. By applying mass balance and continuity equation for each pore and applying two boundary conditions (the pressures on the left and right boundaries are given and are designated as P_{high} and P_{low}, respectively), the internal distribution of pressure is obtained.

The flow rate F_{ij} flowing from a given throat ij that connects pore i with pore j is obtained using:

$$F_{ij} = \frac{\Delta P_{ij}}{R_{ij}} \tag{5}$$

where R_{ij} is the resistance to flow in throat ij that is defined as Eq. (6) ($1/R_{ij}$ represents the resistance of throat ij) and ΔP_{ij} is the pressure difference between two adjacent pores i and j.

$$R_{ij} = \frac{8\mu_l l_{ij}}{\pi r_{ij}^4} \tag{6}$$

where r_{ij} and l_{ij} are the radius and the length of the throat ij, respectively. And μ_l is the dynamic viscosity of liquid that flows through the throat ij.

For incompressible liquid phase, the continuity equation can be written as:

$$\sum_j F_{ij} = 0 \tag{7}$$

where the summation is run for each pore i that is connected to a set of pores indicated by j. Combination of Eqs. (5), (6), and (7) provides a system of algebraic equations as:

$$G \cdot P = b \tag{8}$$

where G is a sparse matrix that contains flow resistance or conductance, P is a vector that contains unknown pressure values, and b is a known vector containing the effect of boundary conditions. A solution of this system provides pressure value in each pore.

2.4 Hydrate dissociation

The hydrate is assumed to be in equilibrium with temperature and pressure of the surrounding environment. The equilibrium pressure can be computed using a procedure based on thermodynamic principles and applying the van der Waals–Platteeuw theory (van der Waals and Platteeuw 1959). In isothermal conditions, with decreasing pressure in the system below the equilibrium pressure, the possibility of hydrate dissociation increases. To change the pressure, its value for one of the boundaries is changed, while the other boundary pressure value is kept unchanged. Pressure perturbation causes hydrate dissociation to produce water and gas. Within the pore network, the pressure of each pore that contains hydrate is compared with equilibrium pressure for dissociation. When the pressure is lower than equilibrium pressure, the dissociation will occur. After the dissociation, we follow percolation step. The Hoshen–Kopelman algorithm is used for percolation step to obtain the clustered pores (Hoshen and Kopelman 1976). In this step, one threshold pressure is defined as Eq. (9).

$$\Pi_{ij} = P_c^{ij} + P_l^j \tag{9}$$

$$P_c^{ij} = \frac{2\sigma}{r_{ij}} \tag{10}$$

where P_c^{ij} is the capillary pressure of the throat between pores i and j, P_l^j is the pressure of pore j, σ is the interfacial tension, and r_{ij} is the radius of the throat ij.

If the gas pressure in a given pore is larger than the summation of capillary pressure of the connected throat and liquid pressure of its adjacent pore (i.e.,$P_g > \Pi ij$), the gas will invade the neighboring water-filled pore. Otherwise, the pore remains water-filled. Pores are filled

with the gas phase in a pore-by-pore order until all pores are occupied. After the invasion, the presence of clustering is possible. As the gas expands, the gas pressure decreases. There are many equations of state to calculate the pressure of gases. In this work, due to qualitative study and reduction in run time, the modified ideal gas law is used to determine the updated pressure of pores in each cluster.

$$P_{\mathrm{g}} = \frac{znRT}{V} \tag{11}$$

where P_{g} is pressure, z is compressibility factor, n is the number of gas moles, R is the gas constant, T is temperature, and V is volume.

2.5 Gas Production Evaluation

Whenever a gas cluster reaches the outlet boundary of the network, it is extracted and the pressure in the gas cluster becomes equal to the external fluid pressure, P_{low}. Gas recovery yield, η, is determined at each clustering step as the ratio of the recovered gas to the initial gas as:

$$\eta = \frac{(n_1 - n_2)}{n_1} * 100 \tag{12}$$

where n_1 and n_2 are the amounts of initial and final gas in the porous medium, respectively. In contrast, if a gas phase does not grow to reach the outlet, it remains within the network as a trapped isolated cluster.

2.6 Angular Throats

The angular cross-sectional shape of throats in the constructed pore network model can improve the simulation accuracy of the multiphase flow (Valvatne and Blunt 2004). Unlike common cylindrical throats in pore networks, both wet and non-wet phases can exist in angular throats (Tuller and Or 2001). Non-wet phase (gas) occupies the center of the throats, and wet phase (water) remains in the corners of the triangle. Under this condition, Eq. (6) cannot be applied directly and it is modified as:

$$R_{ij} = \frac{8B\pi\mu_{\mathrm{l}} l_{ij}}{A_{\mathrm{w},ij}^2} \tag{13}$$

where B is a dimensionless flow resistance factor (equal to 5.3 for equilateral triangular pore throat (Bakke and Øren 1997; Ranshoff and Radke 1988)), $A_{\mathrm{w},ij}$ is the cross-sectional area open to flow for wet phase, and as before μ_{l} and l_{ij} are the dynamic viscosity of fluid and the length of throat ij, respectively. Initially, the whole network is water-filled and the cross section of throat for wetting phase can be calculated as (Bakke and Øren 1997):

$$A_{\mathrm{w}} = \frac{r_{\mathrm{m}}^2}{4S_{\mathrm{f}}} \tag{14}$$

$$S_{\mathrm{f}} = \frac{A}{P^2} \tag{15}$$

where r_{m} is the inscribed radius of the throat, $\mathrm{S_f}$ is the dimensionless shape factor (Eq. 15), A is the area of the pore throat cross section, and P is the corresponding perimeter.

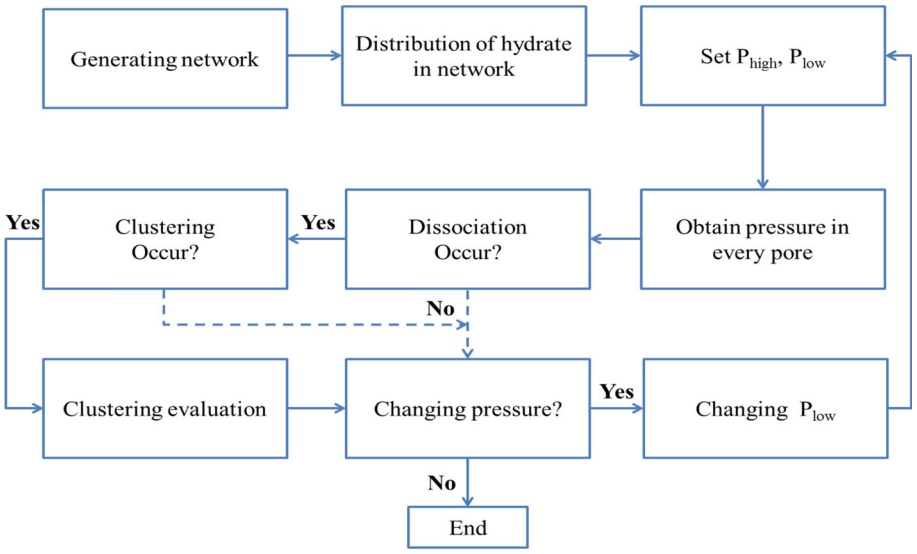

Fig. 3 Block flow diagram of our procedure for investigation of hydrate dissociation

For invading step, the relationship between capillary pressure and the inscribed radius of the throat may be described as:

$$P_c^{ij} = \frac{\sigma\left(1 + 2\sqrt{\pi S_f}\right)}{r_m} \tag{16}$$

The cross-sectional area of wet phase in the angular throat, A_w, can be obtained from Eq. (17) (Tuller et al. 1999).

$$A_w = 3r_m^2 \cdot F(\alpha) \tag{17}$$

$$F(\alpha) = \frac{1}{\tan\left(\frac{\alpha}{2}\right)} - \frac{\pi(180 - \alpha)}{360} \tag{18}$$

where α is angularity of corner and $F(\alpha)$ is a corner angularity factor. In this study, throats with equilateral triangular cross sections were considered.

Figure 3 describes the simulation procedure of hydrate dissociation.

3 Results and Discussion

We have simulated domain sizes of 50×50 pores having a 15% porosity (i.e., the ratio of the pore and throat volumes to the total volume of the network). Each obtained data point in the following figures is an average of 20 realizations. Simulation parameter values relevant to methane hydrate dissociation have been considered, including $T_{eq} = 283.2$ K, $P_{eq} = 6.95$ MPa, $\mu_l = 10^{-3}$ Pa·s, $z = 0.85$, $\sigma = 0.07$ N/m, and $\rho_H = 913.0$ kg/m^3(Smith and Van Ness 1987; Tsimpanogiannis and Lichtner 2006). To present the simulation results, we have defined the dimensionless parameter ΔP_D as the ratio of pressure difference to P_{high}.

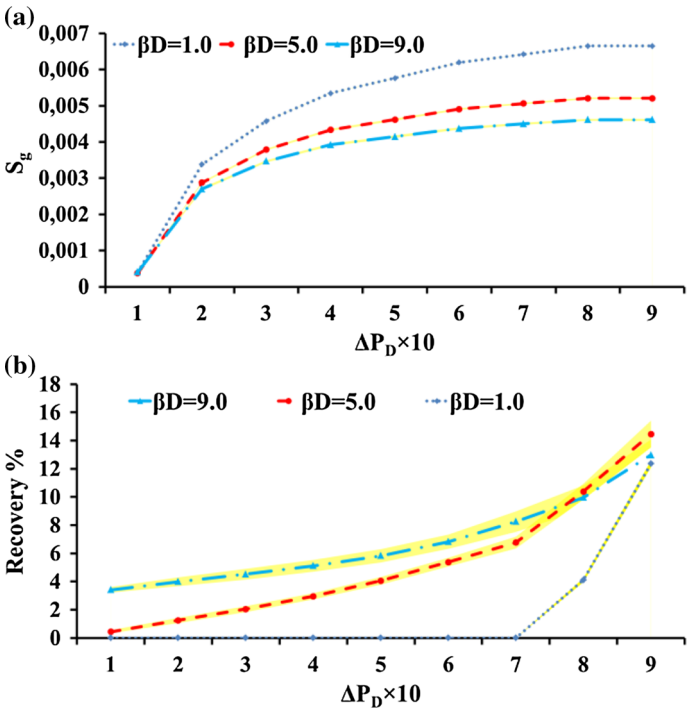

Fig. 4 **a** Gas saturation, **b** recovery percent, as a function of ΔP_D in various β_D, and size of network = 50 × 50, porosity = 15%, initial hydrate saturation = 4%

3.1 Effect of β_D on Gas Saturation and Recovery Percent

To explore the effect of hydrate spatial distribution (i.e., uniform and non-uniform distributions) all other numerical parameters were kept constant except the parameter that is being examined (i.e., β_D). For a fixed hydrate saturation of 4% and a constant pore size distribution, we varied the parameter β_D, to obtain the resulting gas saturation. Figure 4a shows the effect of β_D on the gas saturation. Results show that by increasing β_D (i.e., a more non-uniform distribution of hydrate) the amount of gas saturation decreased for each ΔP_D step.

For lower β_D values most of the pores were hydrated. Under this condition, after altering the pressure, the dissociation phenomena occurred to produce gas in most of locations within the pore network resulting in a high value of gas saturation. In contrast, under higher β_D values the distribution of hydrate in the network is non-uniform which results in a larger number of empty pores. Upon dissociation, the amount of gas is lower compared to the uniform distribution.

Figure 4b demonstrates the recovery percentage (obtained using Eq. 12) from a hydrate system with different β_D values. As can be seen from this figure, by increasing β_D, the recovery percentage also increases. This observation can be explained by examining whether the pressure of the gas in every pore is adequate to overcome the threshold pressure so that the gas phase invades the adjacent pore to create a gas cluster (Fig. 5). In a uniform distribution, the gas pressure of pores cannot overcome the threshold pressure which maintains a low recovery percentage. Figure 4 shows that with increasing ΔP_D, both gas saturation and the recovery percentage increase, which is consistent with previous studies (Jang and Santamarina 2011;

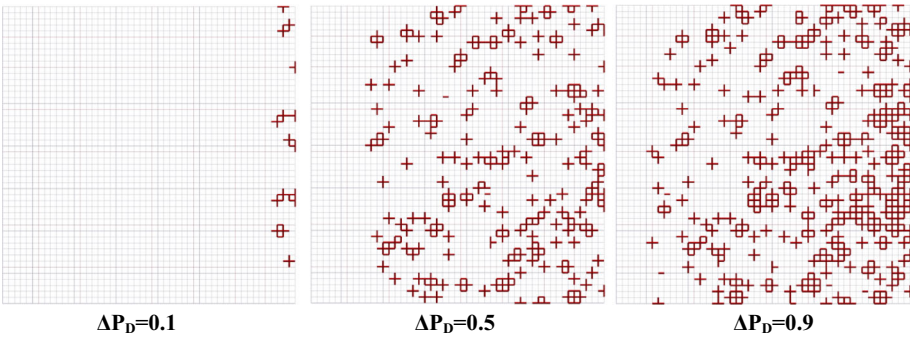

Fig. 5 Clustering in various ΔP_D, and size of network = 50 × 50, porosity = 15%, initial hydrate saturation = 4%, β_D = 9.0. Higher ΔP_D values result in an increase in the gas clustering within the network

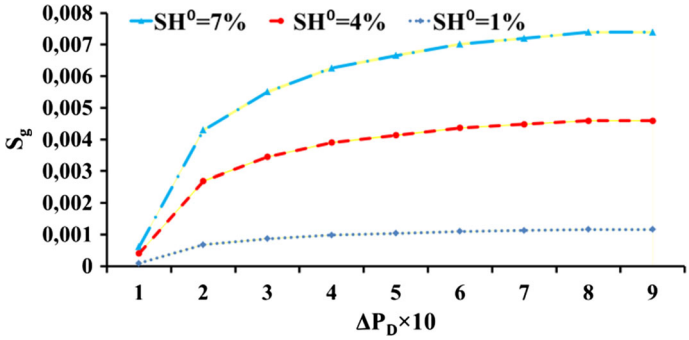

Fig. 6 Gas saturation as a function of ΔP_D in various initial hydrate saturations, and β_D = 9.0, size of network = 50 × 50, porosity = 15%

Tsimpanogiannis and Lichtner 2006). The results are compared with Tsimpanogiannis and Lichtner's (2006) work by plotting the gas saturation as a function of ΔP_D. The trend of our model is the same as that study, and the difference is due to diversity of pore size distribution. Also in the Tsimpanogiannis and Lichtner's work, the depth of network is considered unity, but in our model we assumed twice the maximum radius. So, our results are validated by a comparison with their results.

3.2 Effect of Initial Hydrate Saturation on the Gas Saturation

Natural reservoirs of hydrates in the oceanic porous media contain at least 4–8% hydrate saturation, S_H^0, and at the highest level it would be around 20–30% (Davie and Buffett 2003). The lower limit has been chosen to perform quasi-static simulations. Several initial hydrate saturations were used: S_H^0 = 0.01, 0.04, and 0.07. For each simulation run, all other modeling parameters were kept constant. As predicted, by increasing the initial hydrate saturation in porous media higher gas saturation is achieved (Fig. 6).

3.3 Effect of the Pore and Throat Size Distributions on Gas Saturation

In this section, we have chosen a β_D value of 9.0 and an initial hydrate saturation of 4% to analyze the effect of pore size distribution. As shown in Fig. 7, while the pore size distribution

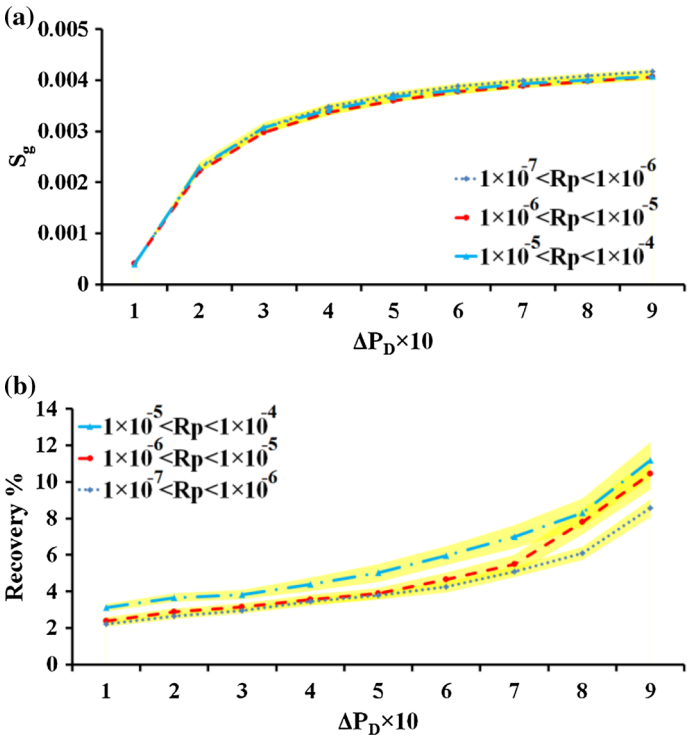

Fig. 7 **a** Gas saturation, **b** recovery percent, as a function of ΔP_{D} for various pore size distributions, for a network size of 50×50, porosity = 15%, $S_{\mathrm{H}}^{0} = 4\%$, $\beta_{\mathrm{D}} = 9.0$

does not have a significant effect on gas saturation it plays a crucial role in the recovery percentage. This behavior can be explained by the fact that an increasing throat radius lowers the entry capillary pressure of the pores. A lower value of entry capillary pressure facilitates the invasion of pores using the gas phase to increase the recovery.

3.4 Effect of Angularity of Throats

Triangular throats, in addition to affecting porosity, can cause additional liquid to be kept at the corners after the invasion by the non-wetting phase (i.e., the gas phase in this study). This phenomenon causes higher connectivity, and therefore, the flow of the liquid wetting phase affects the relative permeability (Fig. 8). The absolute permeability of the whole pore network can be calculated using Darcy's law.

$$F = \frac{kA}{\mu}\frac{\Delta P}{L} \tag{19}$$

where F is flow rate, k is absolute permeability, A is area, μ is dynamic viscosity, and ΔP is pressure drop across the domain L. Throat sizes are chosen so that porosity remains the same (Ebrahimi and Or 2015). Similar to the previous section, a change in pressure causes dissociation and permeability changes. The ratio of the permeability to the absolute permeability is known as relative permeability. Figure 9a depicts the trend of relative permeability for circular and triangular throat cross sections for 2D network. As can be seen from this figure, the relative permeability decreases while ΔP_{D} is increased. In triangular cross section

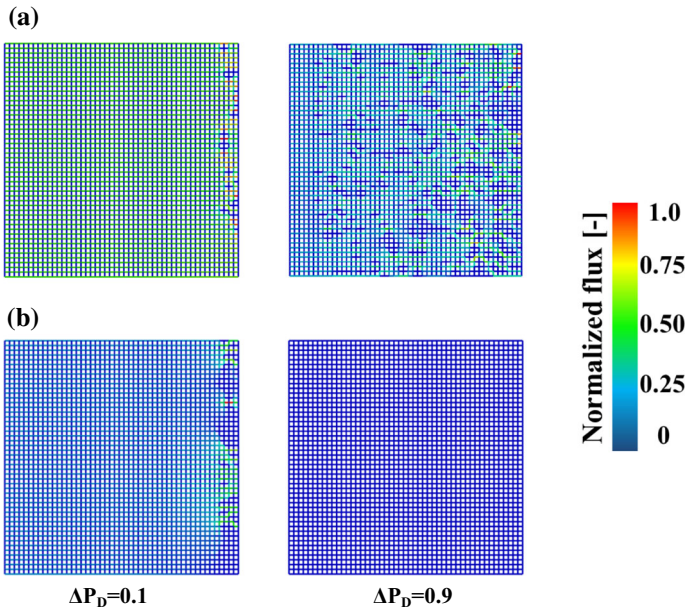

Fig. 8 Distribution of the flow rates in a 2D network of size 50×50 for different ΔP_D values, **a** after dissociation using angular pore throats, as well as **b** after dissociation applying circular throat having no corner flow

of throats, due to water existence in the corners, the reduction is smooth, but using circular pore cross sections, the reduction is sharp as the wetting phase becomes disconnected to eventually force permeability to approach zero. To be able to compare the two models, the sizes of angular pores are chosen so that the entry capillary pressure of pore throats be the same in both circular and angular pore networks. Therefore, the same inscribed radius for the throats in circular and triangular cross sections was applied. As a result, the amount of gas saturation and recovery percentage did not change significantly between the two pore networks (Fig. 9b, c).

3.5 Computations Using 3D and 2D pore Networks

To more accurately represent a real porous media, the algorithm of fluid flow in the 2D pore network model can be extended to the 3D network domains. In this section, two networks (with sizes of 30×30 pores and $30 \times 30 \times 30$ pores) are used to evaluate the effect of network dimension on the efficiency of gas recovery. In 3D network (Fig. 10), due to the higher coordination number (equal to 6) compared to the 2D networks (equal to 4), clusters have more freedom to transport and grow. Therefore, the cluster size and, consequently, the amount of gas recovery in the 3D network are larger compared to the 2D network (Fig. 11). However, because of increasing the number of pores in the 3D network, the computation time is considerably increased. Therefore, 2D networks may be used to understand the process as well as to obtain an approximation for the amount of the recoverable gas.

As shown in Fig. 11c, after $\Delta P_D = 0.6$, the slope is changed. Also, it is clear in Fig. 11b that from $\Delta P_D = 0.6$, the percentage of gas recovery is sharply increased. It may be inferred that for the production of gas from hydrate reservoirs with high recovery percent the ΔP_D should be above 0.6.

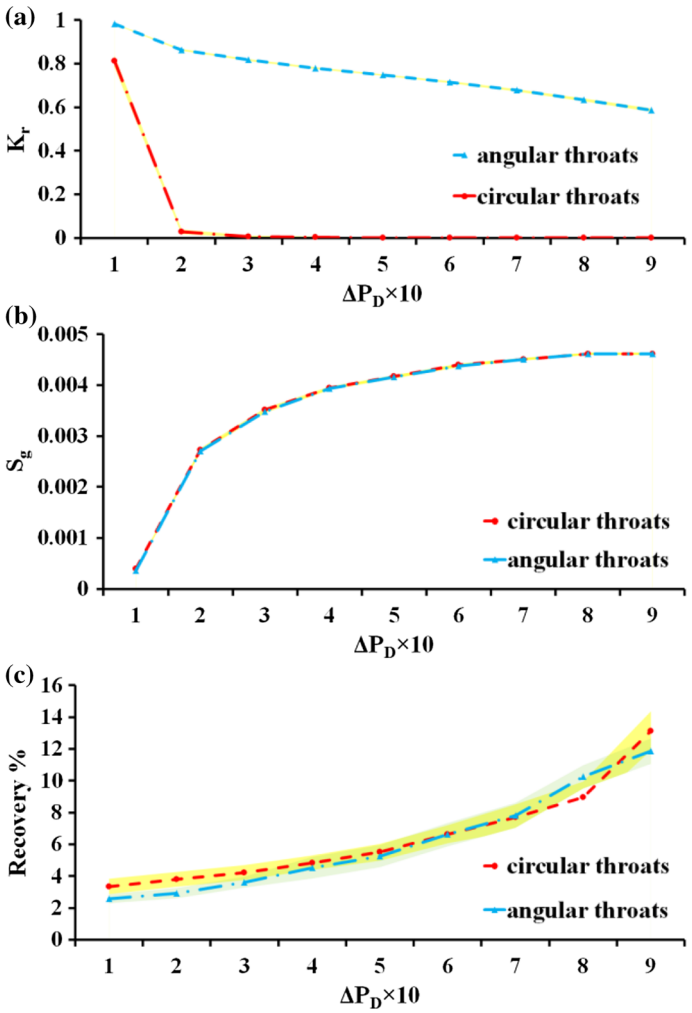

Fig. 9 **a** Relative permeability, **b** the gas saturation, **c** recovery percent, as a function of ΔP_D in angular and circular throat cross sections, and size of network = 50 × 50, porosity = 15%, $S_H^0 = 4\%$, $\beta_D = 9.0$

We made an attempt to obtain a relation between the results obtained from 3D and 2D networks. To do so, several simulations using different-sized pore networks were performed to find a ratio of the gas saturation and recovery percentage in 3D and 2D networks. The gas saturation ratio is defined as the gas saturation for 3D network divided by its value for the 2D network. The results are obtained using a large enough network size. In this case, the network size has no effect on gas saturation. The comparison has shown a linear relation, Eq. (20), for the ratio of recovery percentage of 3D and 2D networks as a function of ΔP_D. This equation provides estimates of three-dimensional gas recovery using 2D network which is much faster computationally.

$$\text{Recovery}\% \left(\frac{3D}{2D}\right) = 1.9170\Delta P_D + 0.9389 \tag{20}$$

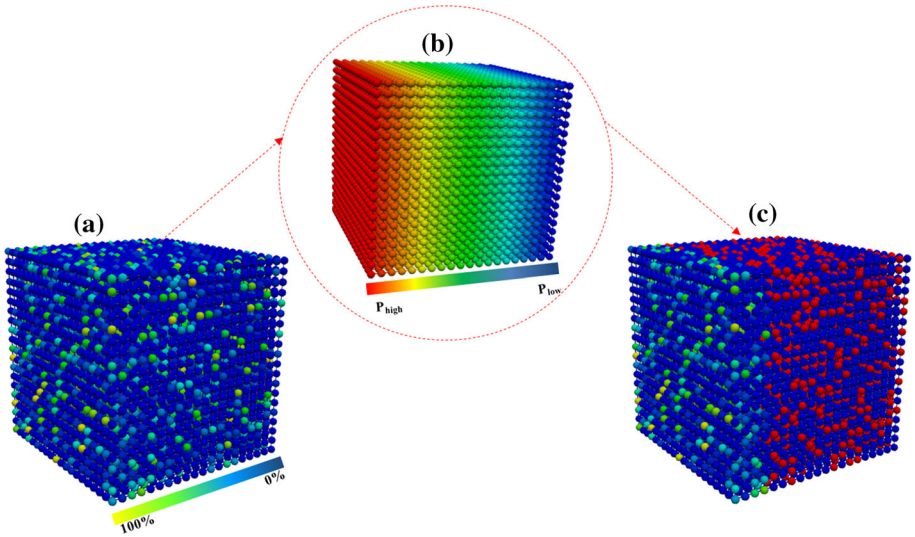

Fig. 10 Schematic representation of 3D network: **a** hydrate distribution, **b** distribution of pressure, **c** gas saturation with un-dissociation hydrate

4 Summary and Conclusion

We presented the effect of hydrate initial value and its distribution in porous media on gas saturation and gas recovery. 2D pore network was used to simulate the depressurization process across the network and the resulting dissociation of hydrate. The results indicate that the gas saturation and recovery percent are considerably influenced by the degree of non-uniformity of hydrate distribution, initial hydrate saturation, and pore size distribution. Particularly, we have found that:

- The amount of gas recovery increases for a heterogeneity system with non-uniform hydrate distribution. Comparably, in the presence of uniform hydrate distribution, gas phase cannot invade a large fraction of the pore spaces. This is because the gas phase from hydrate decomposition cannot overcome the pore's threshold pressure to mobilize the gas phase. In real systems, while the characteristic properties of porous media (e.g., pore size and porosity) can be measured experimentally, the distribution of hydrate cannot be determined easily. The presented model can help to predict the possible range of gas saturation and recovery.
- Our results indicate that increasing the pressure difference across the pore network leads to the growth of gas clusters and the gas recovery. However, the results depict that applying a normalized pressure of larger than 0.6 results in efficient gas recovery.
- Distribution of pore size, which affects the threshold entry pressure of pores, has a major impact on gas invasion, clustering, and eventually recovery efficiency. In the presence of small pore size, the resistance to the movement of gas increases and the generated gas phase cannot easily invade the adjacent pores and grow toward the outlet.
- For rounded pore shapes, only one phase can exist within a pore and water phase can become disconnected. However, in the presence of angular pores, water and methane gas can coexist in a single pore. Flow of water along the corners of the angular pores increases the relative permeability values of the system.

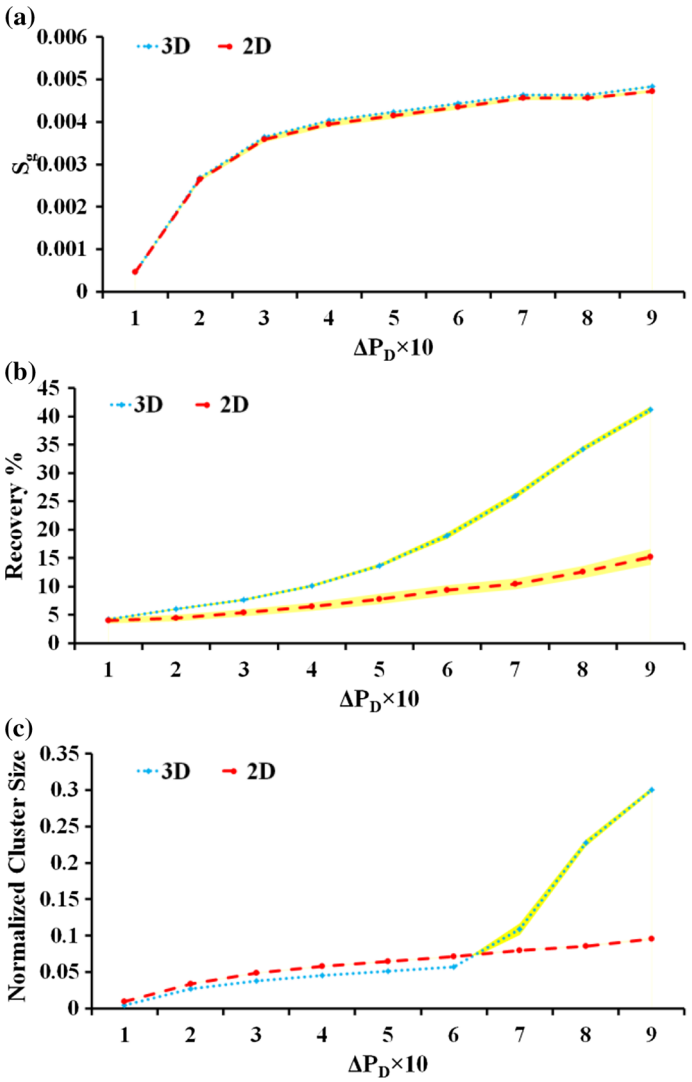

Fig. 11 **a** Gas saturation, **b** recovery percent, **c** normalized cluster size, as a function of ΔP_D in 2D and 3D network, porosity = 15%, $S_H^0 = 4\%$, $\beta_D = 9.0$

- 3D networks enhance pore connectivity to increase the gas clustering and recovery; however, with a predictable trend that can be driven using 2D networks. We have provided a relation for gas recovery of 3D networks based on 2D simulations which considerably lowers computational time.

References

Ai, L., Zhao, J., Wang, J., Song, Y.: Analyzing permeability of the irregular porous media containing methane hydrate using pore network model combined with CT. Energy Proc. **105**, 4802–4807 (2017). https://doi.org/10.1016/j.egypro.2017.03.950

Asif, M., Muneer, T.: Energy supply, its demand and security issues for developed and emerging economies. Renew. Sustain. Energy Rev. **11**, 1388–1413 (2007). https://doi.org/10.1016/j.rser.2005.12.004
Bai, Y., Li, Q., Zhao, Y., Li, X., Du, Y.: The experimental and numerical studies on gas production from hydrate reservoir by depressurization. Transp. Porous Media **79**, 443–468 (2009). https://doi.org/10.1007/s11242-009-9333-1
Bakke, S., Øren, P.-E.: 3-D pore-scale modelling of sandstones and flow simulations in the pore networks. Soc. Pet. Eng. **2**, 136–149 (1997)
Bhade, P., Phirani, J.: Gas production from layered methane hydrate reservoirs. Energy **82**, 686–696 (2015). https://doi.org/10.1016/j.energy.2015.01.077
Boswell, R., Collett, T.S.: Current perspectives on gas hydrate resources. Energy Environ. Sci. **4**, 1206–1215 (2011). https://doi.org/10.1039/C0EE00203H
Cao, M., Gregson, K., Marshall, S.: Global methane emission from wetlands and its sensitivity to climate change. Atmos. Environ. **32**, 3293–3299 (1998). https://doi.org/10.1016/S1352-2310(98)00105-8
Cheng, Y., Li, L., Yuan, Z., Wu, L., Mahmood, S.: Finite element simulation for fluid-solid coupling effect on depressurization-induced gas production from gas hydrate reservoirs. J. Nat. Gas Sci. Eng. **10**, 1–7 (2013). https://doi.org/10.1016/j.jngse.2012.10.001
Cherskii, N.V., Bondarev, E.A.: Thermal method of exploiting gas-hydrated strata. Sov. Phys. Dokl. **17**, 211–213 (1972)
Collett, T.S.: Potential of gas hydrates outlined. Oil Gas J. **90**, 84–87 (1992)
Collett, T.S., Lewis, R., Uchida, T.: Growing interest in gas hydrates. Oilfield Review (2000)
Collett, T., Johnson, A., Knapp, C., Boswell, R.: Natural Gas Hydrates—Energy Resource Potential and Associated Geologic Hazards. American Association of Petroleum Geologists National Energy Technology Laboratory (NETL) AAPG Foundation AAPG Energy Minerals Division (2009)
Collett, T.S., Kuuskraa, V.A.: Hydrates contain vast store of world gas resources. Oil Gas J. **96**, 90–95 (1998)
Dai, S., Seol, Y.: Water permeability in hydrate-bearing sediments: a pore scale study. Geophys. Res. Lett. **41**, 4176–4184 (2014). https://doi.org/10.1002/2014GL060535.Received
Davie, M.K., Buffett, B.A.: A numerical model for the formation of gas hydrate below the seafloor. J. Geophys. Res. Solid Earth. **106**, 497–514 (2001). https://doi.org/10.1029/2000JB900363
Davie, M.K., Buffett, B.A.: Sources of methane for marine gas hydrate: inferences from a comparison of observations and numerical models. Earth Planet. Sci. Lett. **206**, 51–63 (2003). https://doi.org/10.1016/S0012-821X(02)01064-6
Dendy Sloan Jr., E., Koh, C.: Clathrate Hydrates of Natural Gases. CRC Press, Boca Raton (2007)
Dendy Sloan Jr., E.: Clathrate Hydrates of Natural Gases. Marcel Dekker, New York (1998)
Ebrahimi, A., Or, D.: Hydration and diffusion processes shape microbial community organization and function in model soil aggregates. Water Resour. Res. **51**, 9804–9827 (2015)
Englezos, P., Lee, J.D.: Gas hydrates: a cleaner source of energy and opportunity for innovative technologies. Korean J. Chem. Eng. **22**, 671–681 (2005). https://doi.org/10.1007/BF02705781
Han, D., Wang, Z., Song, Y., Zhao, J., Wang, D.: Numerical analysis of depressurization production of natural gas hydrate from different lithology oceanic reservoirs with isotropic and anisotropic permeability. J. Nat. Gas Sci. Eng. (2017). https://doi.org/10.1016/j.jngse.2017.08.015
Holtzman, R., Juanes, R.: Thermodynamic and hydrodynamic constraints on overpressure caused by hydrate dissociation: a pore-scale model. Geophys. Res. Lett. **38**, 1–6 (2011). https://doi.org/10.1029/2011GL047937
Hong, H., Pooladi-Darvish, M.: Simulation of depressurization for gas production from gas hydrate reservoirs. J. Can. Pet. Technol. (2005). https://doi.org/10.2118/05-11-03
Hoshen, J., Kopelman, R.: Percolation and cluster distribution. I. Cluster multiple labeling technique and critical concentration algorithm. Phys. Rev. B. **14**, 3438–3445 (1976). https://doi.org/10.1103/PhysRevB.14.3438
Jang, J., Santamarina, J.C.: Recoverable gas from hydrate-bearing sediments: pore network model simulation and macroscale analyses. J. Geophys. Res. Solid Earth **116**, 1–12 (2011). https://doi.org/10.1029/2010JB007841
Jang, J., Santamarina, J.C.: Evolution of gas saturation and relative permeability during gas production from hydrate-bearing sediments: gas invasion vs. gas nucleation. J. Geophys. Res. Solid Earth **119**, 116–126 (2014). https://doi.org/10.1002/2013JB010480
Kumar, A., Maini, B., Bishnoi, P.R., Clarke, M., Zatsepina, O., Srinivasan, S.: Experimental determination of permeability in the presence of hydrates and its effect on the dissociation characteristics of gas hydrates in porous media. J. Pet. Sci. Eng. **70**, 114–122 (2010). https://doi.org/10.1016/j.petrol.2009.10.005
Li, X.-S., Xu, C.-G., Zhang, Y., Ruan, X.-K., Li, G., Wang, Y.: Investigation into gas production from natural gas hydrate: a review. Appl. Energy **172**, 286–322 (2016). https://doi.org/10.1016/j.apenergy.2016.03.101

Liang, H., Song, Y., Liu, Y., Yang, M., Huang, X.: Study of the permeability characteristics of porous media with methane hydrate by pore network model. J. Nat. Gas Chem. **19**, 255–260 (2010). https://doi.org/10.1016/S1003-9953(09)60078-5

Mahabadi, N., Dai, S., Seol, Y., Sup Yun, T., Jang, J.: The water retention curve and relative permeability for gas production from hydrate-bearing sediments: pore-network model simulation. Geochem. Geophys. Geosyst. **17**, 3099–3110 (2016). https://doi.org/10.1002/2016gc006372

Mahabadi, N., Jang, J.: Relative water and gas permeability for gas production from hydrate-bearing sediments. Geochem. Geophys. Geosyst. **15**, 2346–2353 (2014). https://doi.org/10.1002/2014gc005331

Makogon, Y.F.: Natural gas hydrates—a promising source of energy. J. Nat. Gas Sci. Eng. **2**, 49–59 (2010). https://doi.org/10.1016/j.jngse.2009.12.004

Makogon, Y.F., Holditch, S.A., Makogon, T.Y.: Natural gas-hydrates—a potential energy source for the 21st Century. J. Pet. Sci. Eng. **56**, 14–31 (2007). https://doi.org/10.1016/j.petrol.2005.10.009

Max, M.D., Dillon, W.P.: Oceanic methane hydrate: the character of the Blake Ridge hydrate stability zone, and the potential for methane extraction. J. Pet. Geol **21**, 343–358 (1998). https://doi.org/10.1111/j.1747-5457.1998.tb00786.x

Max, M.D., Lowrie, A.: Oceanic methane hydrates: a "frontier" gas resource. J. Pet. Geol **19**, 41–56 (1996). https://doi.org/10.1111/j.1747-5457.1996.tb00512.x

Merey, S., Sinayuc, C.: Investigation of gas hydrate potential of the Black Sea and modelling of gas production from a hypothetical Class 1 methane hydrate reservoir in the Black Sea conditions. J. Nat. Gas Sci. Eng. **29**, 66–79 (2016). https://doi.org/10.1016/j.jngse.2015.12.048

Mestdagh, T., Poort, J., De Batist, M.: The sensitivity of gas hydrate reservoirs to climate change: perspectives from a new combined model for permafrost-related and marine settings. Earth Sci. Rev. **169**, 104–131 (2017). https://doi.org/10.1016/j.earscirev.2017.04.013

Moridis, G.J., Collett, T.S., Boswell, R., Kurihara, M., Reagan, M.T., Koh, C., Sloan, E.D.: Toward production from gas hydrates: current status, assessment of resources, and simulation-based evaluation of technology and potential. SPE Reserv. Eval. Eng. **12**, 745–771 (2009). https://doi.org/10.2118/114163-PA

Moss, A.R., Jouany, J.P., Newbold, J.: Review article methane production by ruminants: its contribution to global warming. Ann. Zootech. **49**, 231–253 (2000). https://doi.org/10.1051/animres:2000119

Myshakin, E.M., Ajayi, T., Anderson, B.J., Seol, Y., Boswell, R.: Numerical simulations of depressurization-induced gas production from gas hydrates using 3-D heterogeneous models of L-Pad, Prudhoe Bay Unit, North Slope Alaska. J. Nat. Gas Sci. Eng. **35**, 1336–1352 (2016). https://doi.org/10.1016/j.jngse.2016.09.070

Oliveira, E.A., Schrenk, K.J., Araújo, N.A.M., Herrmann, H.J., Andrade, J.S.: Optimal-path cracks in correlated and uncorrelated lattices. Phys. Rev. E Stat. Nonlinear Soft Matter Phys. **83**, 46113 (2011). https://doi.org/10.1103/physreve.83.046113

Paull, C.K., Dillon, W.P. (eds.): Natural gas hydrates: Occurrence, distribution, and detection. American Geophysical Union, Washington, DC (2001)

Ranshoff, T.C., Radke, C.J.: Laminar Flow of a Wetting Liquid Along the Corners of a Predominantly Gas-occupied Noncircular Pore. J. Colloid Interface Sci. **121**, 392–401 (1988)

Reagan, M.T., Moridis, G.J., Johnson, J.N., Pan, L., Freeman, C.M., Pan, L., Boyle, K.L., Keen, N.D., Husebo, J.: Field-scale simulation of production from oceanic gas hydrate deposits. Transp. Porous Media **108**, 151–169 (2015). https://doi.org/10.1007/s11242-014-0330-7

Ruppel, C.D., Kessler, J.D.: The interaction of climate change and methane hydrates. Rev. Geophys. **55**, 126–168 (2017). https://doi.org/10.1002/2016RG000534

Shafiee, S., Topal, E.: When will fossil fuel reserves be diminished? Energy Policy **37**, 181–189 (2009). https://doi.org/10.1016/j.enpol.2008.08.016

Smith, J.M., Van Ness, H.C.: Introduction to Chemical Engineering Thermodynamics. McGraw-Hil, New York (1987)

Sun, X., Nanchary, N., Mohanty, K.K.: 1-D modeling of hydrate depressurization in porous media. Transp. Porous Media **58**, 315–338 (2005). https://doi.org/10.1007/s11242-004-1410-x

Tsimpanogiannis, I.N., Lichtner, P.C.: Pore-network study of methane hydrate dissociation. Phys. Rev. E Stat. Nonlinear Soft Matter Phys. **74**, 1–13 (2006). https://doi.org/10.1103/physreve.74.056303

Tsimpanogiannis, I.N., Lichtner, P.C.: Gas saturation resulting from methane hydrate dissociation in a porous medium: comparison between analytical and pore-network results. J. Phys. Chem. C **117**, 11104–11116 (2013). https://doi.org/10.1021/jp400449g

Tuller, M., Or, D.: Hydraulic conductivity of variably saturated porous media: film and corner flow in angular pore space. Water Resour. Res. **37**, 1257–1276 (2001). https://doi.org/10.1029/2000WR900328

Tuller, M., Or, D., Dudley, L.M.: Adsorption and capillary condensation in porous media: liquid retention and interfacial configurations in angular pores. Water Resour. Res. **35**, 1949–1964 (1999). https://doi.org/10.1029/1999WR900098

Uchida, T., Ebinuma, T., Takeya, S., Nagao, J., Narita, H.: Effects of pore sizes on dissociation temperatures and pressures of methane, carbon dioxide, and propane hydrates in porous media. J. Phys. Chem. B. **106**, 820–826 (2002). https://doi.org/10.1021/jp012823w

Valvatne, P.H., Blunt, M.J.: Predictive pore-scale modeling of two-phase flow in mixed wet media. Water Resour. Res. (2004). https://doi.org/10.1029/2003wr002627

van der Waals, J.H., Platteeuw, J.C.: Clathrate Solutions. Presented at the (1959)

Xu, W., Ruppel, C.: Predicting the occurrence, distribution, and evolution of methane gas hydrate in porous marine sediments. J. Geophys. Res. Solid Earth **104**, 5081–5095 (1999). https://doi.org/10.1029/1998JB900092

Zhao, J., Yu, T., Song, Y., Liu, D., Liu, W., Liu, Y., Yang, M., Ruan, X., Li, Y.: Numerical simulation of gas production from hydrate deposits using a single vertical well by depressurization in the Qilian Mountain permafrost, Qinghai-Tibet Plateau, China. Energy **52**, 308–319 (2013). https://doi.org/10.1016/j.energy.2013.01.066